DOI: 10.1002/ejic.201000474

A Single-Source Co/Li/O Organometallic Precursor for Nanocrystalline $LiCoO_2$ – Synthesis, Formation Pathway, and Electrochemical Performance

Jayaprakash Khanderi[a] and Jörg J. Schneider*[a]

Dedicated to Prof. Dr. Jürgen Heck on the occasion of 60th birthday

Keywords: Nanoparticles / Electrochemistry / Cobalt / Lithium / Single-source precursors

A single-source precursor route to phase-pure $LiCoO_2$ by employing the organometallic precursor $[(COD)_2CoLi(thf)_2]$ (**1**) to introduce a Co/Li/O 1:1:2 stoichiometry is described for the first time. Compound **1** undergoes decomposition in the presence of oxygen, forming nanoscaled, electrochemically active $LiCoO_2$ starting at a temperature as low as 200 °C. Its temperature-dependent formation pathway was studied by various spectroscopic and microscopic techniques. The transition temperature for the evolution of layered $LiCoO_2$ is above 400 °C. Electrochemical studies indicate that the low-temperature modification of $LiCoO_2$ can be obtained at 500 °C, showing moderate electrochemical battery performance.

Introduction

$LiCoO_2$ is an established cathode material in lithium ion batteries.[1] Several key properties such as high voltage (ca. 3.8 V), high specific capacity (ca. 180 W h/kg), good rate capability, good cycling stability, and structural stability towards repeated intercalation/deintercalation processes during charge/discharge cycles are its outstanding properties.[2] From a synthetic point of view, the electrochemical properties of $LiCoO_2$ as well as the intercalation materials (Fe, Ni, Mn) are known to be strongly dependent on the synthesis methods and conditions and their subsequent post-processing.[3] The synthesis procedure usually determines to a huge extent purity, structural integrity, particle size, and morphology, hence the final electrochemical performance of $LiCoO_2$ as cathode material. The inherent low conductivity of $LiCoO_2$, necessitates the use of its nanoparticulate form in order to achieve shorter diffusion length and higher surface areas. Any controlled tailoring of such properties depends on an understanding of the formation pathway leading to its formation.[4]

So far, synthesis of $LiCoO_2$ powders and nanoparticles has been achieved by chimie douce solution-based routes, by rf-sputtering,[5] and by high-temperature solid-state routes. Former methods include hydrothermal processing,[6] microwave-assisted synthesis,[7] or sol–gel techniques.[8] Latter techniques use co-precipitation[9] and direct solid-state reactions of powders by high-temperature firing.[10,11] Here, precursor compounds for $LiCoO_2$ are traditional inorganic/organic salts or oxides of lithium and cobalt [e.g., for Li: Li_2O, Li_2CO_3, $LiOOCCH_3$, and LiOH; for Co: $CoCl_2$, $Co(OOCCH_3)_2$, $Co(NO_3)_2$, Co_3O_4, and $CoCO_3$], either in the presence or in the absence of solvents or additional additives.

Typically, ex situ mixing of precursors is required in both approaches to prepare "reactive pre-mixtures", from which the formation of $LiCoO_2$ has to be achieved, often under hardly controllable methods. Due to the multicomponent steps involved in these reactions, the chemical composition and structure of the intermediates in the individual process steps are not known,[7] thus a detailed understanding of $LiCoO_2$ formation and morphology evolution is often lacking. Organometallic chemistry allows overcoming the problem associated with multicomponent precursor approaches, since it offers kinetically attractive decomposition routes at moderate temperatures and allows controlling the element stoichiometry precisely.

To the best of our knowledge, no approach using a single-source organometallic precursor containing all constituent atoms for obtaining phase-pure, nanocrystalline, electroactive $LiCoO_2$ has been reported so far. Herein, we report on the synthesis and elucidation of the formation mechanism of nanocrystalline $LiCoO_2$ by using the single-source organometallic precursor [bis(η-1,5-cyclooctadiene)-cobaltlithium] (**1**, containing Li, Co, O at the exact 1:1:2 atomic ratio).

[a] Fachbereich Chemie, Eduard-Zintl-Institut, Anorganische Chemie, Technische Universität Darmstadt,
Petersenstr. 18, 64287 Darmstadt, Germany
Fax: +49-6151-16-3470
E-mail: joerg.schneider@ac.chemie.tu-darmstadt.de

Supporting information for this article is available on the WWW under http://dx.doi.org/10.1002/ejic.201000474.

 © 2010 Wiley-VCH Verlag GmbH & Co. KGaA, Weinheim View this journal online at wileyonlinelibrary.com

Results and Discussion

Compound **1** can be formed by a reductive elimination route from $[(C_5H_5)_2Co(1,5\text{-COD})]$, and Li in thf, as reported by Jonas et al.[12] We performed the controlled decomposition of crystalline, air-sensitive **1**: (a) under an inert atmosphere and (b) under oxygen, to elucidate its detailed decomposition and formation pathway to nanocrystalline $LiCoO_2$ (Scheme 1).

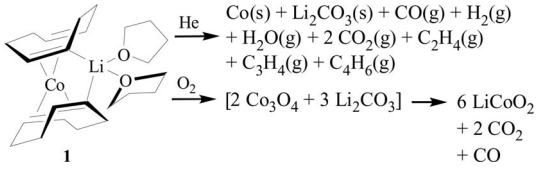

Scheme 1. Decomposition pathways of **1** in helium and in oxygen, leading to $LiCoO_2$ in oxygen.

Thermogravimetric analysis coupled with mass spectrometry (TG/MS) of **1** under flowing He (heating rate 10 °C/min) reveals the loss and decomposition of thf and 1,5-cyclooctadiene (COD) ligands. The first mass loss occurs between 50 and 125 °C (Δm = –52%), and a second one takes place between 130 and 230 °C (Δm = –73%) (Figure 1). Thereafter, an additional mass loss of only 7% was observed up to 600 °C ($\Delta m_{obtained}$ = –80% vs. Δm_{calc} = –83.4%), alluding to near-quantitative formation of metallic Co and Li_2CO_3 under inert conditions.

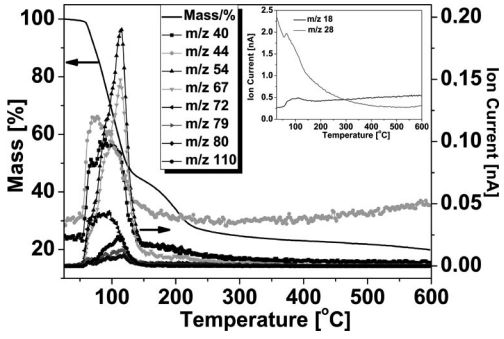

Figure 1. TG/MS of **1**. Inset: MS (ion current profile) of fragments with *m*/*z* 18 and 28.

Simultaneously, mass spectra of the gaseous decomposition products are due to fragmentation of the 1,5-COD ligands: *m*/*z* = 18 (H_2O), 28 (CO/C_2H_4), 40 (C_3H_4), 44 (CO_2), 54 (C_4H_6), 67 (C_5H_8), 72 (thf), 79, 80 (C_6H_8), 110 (C_8H_{14}). These observations are further confirmed by determining the C, H content of composition "$LiCoO_2$" obtained at temperatures between 200–500 °C (see Table S1 in the Supporting Information). The C content decreases from 21.94% at 200 °C (a decrease of more than 70% of **1**) to as low as 1.83% at 500 °C (Table S1).

Following the formation of crystalline Li_2CO_3 by X-ray powder diffraction under (a) anaerobic conditions and (b) at variable temperatures (200°–500 °C) under oxidative conditions allows to elucidate the formation pathway of electroactive $LiCoO_2$ from **1** further (Figure 2a–e). At 200 °C, $LiCoO_2$ formation starts with an amorphous phase. Under anaerobic conditions, metallic cobalt [JCPDS card No. 15–806] and Li_2CO_3 [JCPDS card No. 22-1141] are the sole products of the complete decomposition of **1** at 500 °C, as revealed by X-ray diffraction analysis, which confirms our TGA/MS studies (Figure 2a). Heating **1** under oxidative conditions (O_2) results in the formation of $LiCoO_2$ [Card No. 44-145] and Li_2CO_3, revealed by the evolution of the corresponding X-ray diffraction signals of both phases (see Figure 2, spectra c and d). Formation of the phase-pure $LiCoO_2$ as main product is observed to start at 400 °C. Its formation is connected with the transformation of the intermediate, low-temperature $LiCoO_2$ phase[13] and is evidenced by a splitting of the Bragg peaks at 2θ = 22.2 and 70.5° [see Figure S1a, b in the Supporting Information]. Even though trace amounts of Li_2CO_3 are formed during the decomposition of **1** under oxygen, its presence was found to be beneficial for cell operation, since it can prevent overcharging.[14]

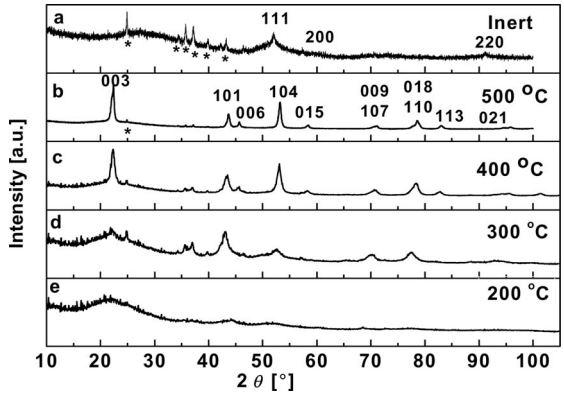

Figure 2. X-ray diffraction patterns (Co-$K_{\alpha 1}$) of $LiCoO_2$ formed by decomposition of **1** (a) in the absence of oxygen at 500 °C and in the presence of oxygen at (b) 500, (c) 400, (d) 300, (e) 200 °C (* denotes Li_2CO_3).

Temperature-dependent evolution of $LiCoO_2$ has been followed by Raman spectroscopy (see Figure S2 in the Supporting Information for spectra and detailed band assignment). Characteristic O–Co–O E_g bending and Co–O A_{1g} stretching modes are observed. The redshift in both absorptions compared to that of the bulk $LiCoO_2$ phase is in accord with the effect of decreasing crystallite size, when going from the bulk to the nanophase.[4,15]

In the X-ray photoelectron survey spectrum of $LiCoO_2$ derived from **1** (500 °C), signatures corresponding to C, O, Co, and Li (see Figure S3 in the Supporting Information) were found. The C 1s peak centered at 284.5 eV (Figure 3a) can be assigned to graphitic carbon,[15] whereas the C 1s peak at 288.9 eV, with an associated shoulder at 287.7 eV, is in accord with an assignment to polymeric type carbon (with a C–C and C–O backbone) associated with lithium.[16,17] The deconvoluted O 1s signals at 529.5 and 530.8 eV have approximately the same intensity (Figure 3b): The signal at 529.5 eV corresponds to O^{2-} ions of the $LiCoO_2$ structure, whereas the one at 530.8 eV (Figure 3b) corresponds to oxygen associated with polymeric type carbon.[17] The Co 2p3/2 peak at 779.8 eV and the Co 2p1/2

 © 2010 Wiley-VCH Verlag GmbH & Co. KGaA, Weinheim

peak at 794.8 eV correspond to the oxidation state Co^{3+} characteristic for $LiCoO_2$ (Figure 3c). The Li 1s signal for L^{1+} is at 54.1 eV (Figure 3d).

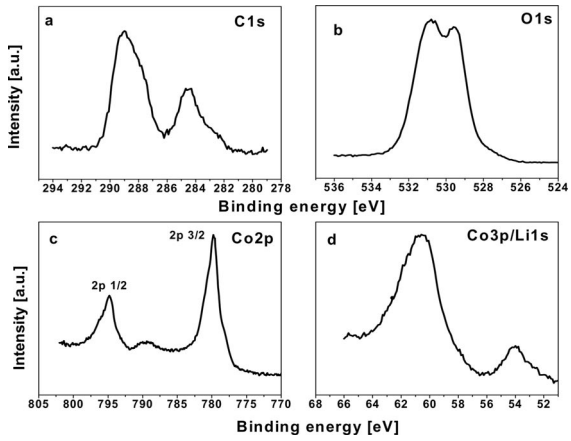

Figure 3. XPS spectra of $LiCoO_2$ synthesized from **1** at 500 °C: (a) C 1s; (b) O 1s; (c) Co 2p; (d) Li 1s and Co 3p.

High-resolution transmission electron microscopy (HRTEM) micrographs of $LiCoO_2$ synthesized from **1** under oxidative conditions at 200 °C and 500 °C are shown in Figure 4. For both synthesis temperatures, the $LiCoO_2$ nanoparticles are crystalline with approximately the same narrow particle distribution of 2–4 nm. $LiCoO_2$ particles are typically agglomerated into smaller clusters of several individual particles.

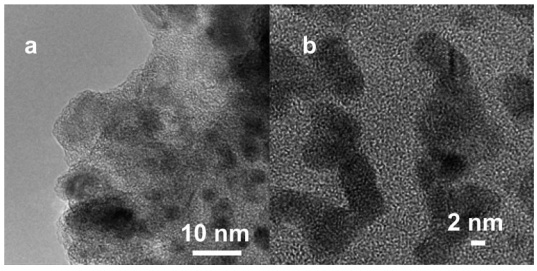

Figure 4. HRTEM images of $LiCoO_2$ powder synthesized under oxidizing conditions at (a) 200 °C and (b) at 500 °C.

Our combined spectroscopic and microscopic studies reveal a complete picture of the formation mechanism of $LiCoO_2$ starting from the molecular precursor **1**. During decomposition of **1** between 200–500 °C in the absence of oxygen, the solid products, nanocrystalline Co and Li, are formed (see TG-MS studies). $H_2O/CO/CO_2$ vapors formed during the decomposition of **1** can then react with Li metal to form Li_2CO_3 as the end product of this decomposition under inert conditions (by reaction of LiOH with CO_2). Thermal decomposition of the COD ligand of **1** might be the source of amorphous and polymeric carbon, which graphitizes at higher temperature (see XPS discussion and Table S1 in the Supporting Information for data on C content). This outer carbon layer prevents further particle coarsening, resulting in an inhibited particle growth over the temperature regime 200–500 °C. Oxygen diffuses through this carbon layer, forming spinel-type cobalt oxide (e.g., Co_3O_4) or $Li_xCo_{1-x}[Co]_2O_4$.[13] Then, either finely divided Co_3O_4 reacts with Li_2CO_3 or conversion of $Li_xCo_{1-x}[Co]_2O_4$ at temperatures above 300 °C occurs to form the final product, $LiCoO_2$. It should be noted that recent reports suggest that meso- or macroporous carbon shells encapsulating electroactive material enhances its cycling performance, reversibility, and rate performance in lithium ion batteries.[18]

Electrochemical measurements were performed on $LiCoO_2$ nanoparticles synthesized from **1** at 200 °C and 500 °C. The material obtained at 200 °C showed very poor electrochemical activity (see Figure S4 in the Supporting Information), indicating low intercalation behavior due to an incomplete formation of the layered structure. However, for the $LiCoO_2$ layered material obtained at 500 °C, the first discharge/charge cycle is > 0.1 e, now indicating good intercalation behavior, thus charging properties (Figure 5a).[7] The initial discharge capacity is 60 mAh/g (Figure 5b). An overall capacity loss of approximately 0.3 mAh/g per cycle is observed, and this may be attributable to the nanoparticulate structure, well in accord with reports on $LiCoO_2$ having 8 nm particle size, prepared by a hydrothermal method, which shows a drastic capacity loss.[4] Furthermore, the $LiCoO_2$ product obtained at 300 °C was then annealed to 750 °C, in order to obtain a morphology of completely layered-type $LiCoO_2$, which is known to exhibit a better electrochemical performance. The electrochemical analysis of this product, however, showed a drastic decrease in capacity [0.35 mAh/g] in comparison to the $LiCoO_2$ obtained at the originally employed lower processing temperatures of 500 °C. It has been reported that $LiCoO_2$ formed at 200 °C under hydrothermal conditions and finally annealed to 900 °C showed a similar reduced electrochemical performance relative to that prepared at lower temperatures, e.g. 700 °C.[19] This is completely in line with our observations and implies that higher temperatures are obviously detrimental to the nanostructured-phase material, having a negative influence on the electrochemical performance of the resulting high-temperature $LiCoO_2$ phase.[19]

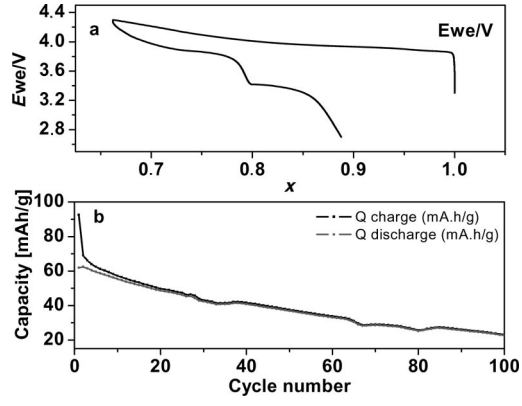

Figure 5. (a) Li^+ vs. potential and (b) charge and discharge capacity vs. cycle number of $LiCoO_2$ synthesized at 500 °C.

 © 2010 Wiley-VCH Verlag GmbH & Co. KGaA, Weinheim

Conclusions

By introducing bis(η-1,5-cyclo-ocatadiene)cobaltlithium (**1**) with Co/Li/O stoichiometric ratio 1:1:2 as single-source precursor, we have demonstrated that electrochemically active nanocrystalline $LiCoO_2$ is accessible. Due to the controlled and clean decomposition pathway under moderate conditions, formation of the electroactive layered-phase $LiCoO_2$ from **1** could be demonstrated. In addition to the formation of $LiCoO_2$ from **1**, our approach is of more general importance for Ni and Fe layered oxides, since organometallic complexes similar to **1**, with a Ni(Fe)/Li stoichiometry of 1:1 are accessible[20] and show thermal behavior comparable to **1**.

Supporting Information (see footnote on the first page of this article): Experimental details, C and H contents, X-ray powder diffraction patterns, Raman and X-ray photoelectron spectra, and electrochemical activity plot.

Acknowledgments

Our work is supported by the Deutsche Forschungsgemeinschaft (DFG) through the Priority program SPP 1181 Nanomaterials. We acknowledge the technical support of Dr. E. Ionescu (Raman), Dr. K. Hofmann (XRD), Dr. N. N. Bramnik, A. Bhasker (electrochemical measurements), Dr. R. W. Hoffman (TG-MS), Dr. A. Issanin (XPS), and Dr. J. Engstler (TEM) during the measurements. Our TEM studies at the Ernst-Ruska Centre for Electron Microscopy, ERC Jülich, were made possible through the ERC1-TUD program.

[1] J. B. Goodenough, Y. Kim, *Chem. Mater.* **2010**, *22*, 587–603; F. Cheg, Z. Tao, J. Liang, J. Chen, *Chem. Mater.* **2008**, *20*, 667–681; A. Yoshino, *Mol. Cryst. Liq. Cryst.* **2000**, *340*, 425–429.
[2] D. Kramer, G. Ceder, *Chem. Mater.* **2009**, *21*, 3799–3809; M. Armand, J. M. Tarascon, *Nature* **2008**, *451*, 652–657.
[3] R. Alacántara, P. Lavela, J. L. Tirado, E. Zhecheva, R. Stoyanova, *J. Solid State Electrochem.* **1999**, *3*, 121–134; J. P. Pereira-Ramos, S. Bach, J. Farcy, N. Baffier, *Ionics* **1997**, *3*, 223–228; T. Bak, J. Nowotny, M. Rekas, C. C. Sorrell, S. Sugihara, *Ionics* **2000**, *6*, 92–106.
[4] Y. Wang, G. Guo, *Adv. Mater.* **2008**, *20*, 2251–2269; M. G. Kim, J. Cho, *Adv. Funct. Mater.* **2009**, *19*, 1497–1514.
[5] J. F. Whitacre, W. C. West, E. Brandon, B. V. Ratnakumar, *J. Electrochem. Soc.* **2001**, *148*, A1078–A1084.
[6] M. Okubo, E. Hosono, J. Kim, M. Enomoto, N. Kojima, T. Kudo, H. Zhou, I. Honma, *J. Am. Chem. Soc.* **2007**, *129*, 7444–7452; X. Qian, X. Cheng, Z. Wang, X. Huang, R. Guo, D. Mao, C. Chang, W. Song, *Nanotechnology* **2009**, *20*, 115608–115614; A. Burukhin, O. Brylev, P. Hany, B. R. Churagulov, *Solid State Ionics* **2002**, *151*, 259–263.
[7] S. Balaji, D. Mutharasu, N. S. Subramanian, K. Ramanathan, *Ionics* **2009**, *15*, 765–777.
[8] S. G. Kang, S. Y. Kang, K. S. Ryu, S. H. Chang, *Solid State Ionics* **1999**, *120*, 155–161; H. Liu, Y. P. Wu, E. Rahm, R. Holze, H. Q. Wu, *J. Solid State Electrochem.* **2004**, *8*, 450–466.
[9] H. Chen, X. Qiu, W. Zhu, P. Hagenmuller, *Electrochem. Commun.* **2002**, *4*, 488–491.
[10] B. Huang, Y. I. Jang, Y. M. Chiang, D. R. Sadoway, *J. Appl. Electrochem.* **1998**, *28*, 1365–1369.
[11] O. A. Shlyaktin, Y. S. Yoon, Y. J. Oh, *J. Eur. Ceram. Soc.* **2003**, *23*, 1893–1899; C. Shao, N. Yu, Y. Liu, R. Mu, *J. Phys. Chem. Solids* **2006**, *67*, 1423–1426.
[12] K. Jonas, R. Mynott, C. Krüger, J. C. Sekutowski, Y. H. Tsay, *Angew. Chem.* **1976**, *88*, 808–809; *Angew. Chem. Int. Ed. Engl.* **1976**, *15*, 767–768.
[13] X. S. Horn, S. A. Hackney, A. J. Kahaian, M. M. Thackeray, *J. Solid State Chem.* **2002**, *168*, 60–68.
[14] K. Ozawa, *Solid State Ionics* **1994**, *69*, 212.
[15] M. Okubo, E. Hosono, T. Kudo, H. S. Zhou, I. Honma, *J. Phys. Chem. Solids* **2008**, *69*, 2911–2915.
[16] M. S. Bhuvaneswari, N. N. Bramnik, D. Ensling, H. Ehrenberg, W. Jaegermann, *J. Power Sources* **2008**, *180*, 553–560.
[17] A. Nytén, M. Stjerndhal, H. Rensmo, H. Siegbahn, M. Armand, T. Gustafsson, K. Edström, J. O. Thomas, *J. Mater. Chem.* **2006**, *16*, 3483–3488.
[18] Y.-S. Hu, P. Adelhelm, B. M. Smarsly, S. Hore, M. Antonietti, J. Maier, *Adv. Funct. Mater.* **2007**, *17*, 1873–1878.
[19] M. Jo, Y.-S. Hong, J. Choo, J. Cho, *J. Electrochem. Soc.* **2009**, *156*, A430–A434.
[20] K. Jonas, *Angew. Chem.* **1975**, *87*, 809–810; *Angew. Chem. Int. Ed. Engl.* **1975**, *14*, 752–753; B. Bogdanovic, M. Kröner, G. Wilke, *Liebigs Ann. Chem.* **1966**, *699*, 1; K. Fischer, K. Jonas, G. Wilke, *Angew. Chem.* **1973**, *85*, 620–621; *Angew. Chem. Int. Ed. Engl.* **1973**, *12*, 565–566.

Received: April 28, 2010
Published Online: September 2, 2010
Publication delayed on authors' request

 © 2010 Wiley-VCH Verlag GmbH & Co. KGaA, Weinheim